Journal of Biotechnology 198 (2015) 3–14

Contents lists available at ScienceDirect

Journal of Biotechnology

journal homepage: www.elsevier.com/locate/jbiotec

Classification of phenotypic subpopulations in isogenic bacterial cultures by triple promoter probing at single cell level

Jan-Philip Schlüter[a], Peter Czuppon[b], Oliver Schauer[a], Peter Pfaffelhuber[b], Matthew McIntosh[a,*], Anke Becker[a,*]

[a] LOEWE Center for Synthetic Microbiology and Faculty of Biology, Philipps-University Marburg, Marburg, Germany
[b] Department of Mathematical Stochastics, Faculty of Mathematics and Physics, Albert-Ludwigs University Freiburg, Freiburg im Breisgau, Germany

ARTICLE INFO

Article history:
Received 30 November 2014
Received in revised form 17 January 2015
Accepted 26 January 2015
Available online 3 February 2015

Keywords:
Phenotypic heterogeneity
Single cell gene expression monitoring
Sinorhizobium meliloti
Exopolysaccharide biosynthesis
Quorum sensing

ABSTRACT

Phenotypic heterogeneity, defined as the unequal behavior of individuals in an isogenic population, is prevalent in microorganisms. It has a significant impact both on industrial bioprocesses and microbial ecology. We introduce a new versatile reporter system designed for simultaneous monitoring of the activities of three different promoters, where each promoter is fused to a dedicated fluorescent reporter gene (*cerulean*, *mCherry*, and *mVenus*). The compact 3.1 kb triple reporter cassette can either be carried on a replicating plasmid or integrated into the genome avoiding artifacts associated with variation in copy number of plasmid-borne reporter constructs. This construct was applied to monitor promoter activities related to quorum sensing (*sinI* promoter) and biosynthesis of the exopolysaccharide galactoglucan (*wgeA* promoter) at single cell level in colonies of the symbiotic nitrogen-fixing alphaproteobacterium *Sinorhizobium meliloti* growing in a microfluidics system. The T5-promoter served as a constitutive and homogeneously active control promoter indicating cell viability. *wgeA* promoter activity was heterogeneous over the whole period of colony development, whereas *sinI* promoter activity passed through a phase of heterogeneity before becoming homogeneous at late stages. Although quorum sensing-dependent regulation is a major factor activating galactoglucan production, activities of both promoters did not correlate at single cell level. We developed a novel mathematical strategy for classification of the gene expression status in cell populations based on the increase in fluorescence over time in each individual. With respect to galactoglucan biosynthesis, cells in the population were classified into non-contributors, weak contributors, and strong contributors.

1. Introduction

The ability of clonal cell populations to split into subtypes displaying different phenotypes is a widespread phenomenon among prokaryotes that has recently intrigued the scientific community. Impact and causative mechanisms of this diversification have attracted much research focus (Casadesús and Low, 2013; Dhar and McKinney, 2007; Maisonneuve and Gerdes, 2014). It contributes to survival strategies at population level, such as bet-hedging, which is the pre-adaptation of subpopulations to unforeseeable environmental changes (Beaumont et al., 2009; Ratcliff and Denison, 2010, 2011; Solopova et al., 2014; Veening et al., 2008). Other benefits may arise from division of labor, as has been reported for pathogenic interactions with a host (Stewart and Cookson, 2012). A paradigmatic example is the bistable expression of virulence genes in *Salmonella typhimurium* resulting in phenotypically virulent and phenotypically avirulent subpopulations which divide labor during infections (Arnoldini et al., 2014). Further examples are the occurrence of persister cells (Helaine and Kugelberg, 2014) and cell differentiation such as spore formation (Veening et al., 2005, 2006). Phenotypic variation may also have a significant impact on the success of industrial bioprocesses as has been indicated by pilot studies in the biotechnological workhorse *Corynebacterium glutamicum* (Frunzke et al., 2008; Neumeyer et al., 2013) and by uncovering the role of phenotypic heterogeneity during various bacterial lag phases (Solopova et al., 2014).

The ability of a given cell type to found a new population again comprising all subtypes implies that individual differences in gene expression or gene product activities rather than alterations in the genome sequence account for such phenotypic heterogeneity. Mechanisms frequently involve variation in gene expression, either caused by fluctuations in intrinsic or environmental factors (Casadesús and Low, 2013; Stewart and Franklin, 2008).

* Corresponding authors.
E-mail addresses: matthew.mcintosh@synmikro.uni-marburg.de (M. McIntosh), anke.becker@synmikro.uni-marburg.de (A. Becker).

http://dx.doi.org/10.1016/j.jbiotec.2015.01.021
0168-1656/

A prominent example for adaptation of subpopulations to microenvironmental variations is bacterial life in biofilms, where non-uniform spatial patterns of properties such as growth rate, respiratory activity, and gene expression have been reported (Huang et al., 1998, 1995; Serra and Hengge, 2014; Wentland et al., 1996).

Single cell analysis techniques including live cell microscopy and flow cytometry are vital to studies of microbial phenotypic variation. Applications of fluorescent reporter proteins paved the way to gene expression studies at the single cell level and provided unprecedented insights into bacterial populations (Chai et al., 2008; Anetzberger et al., 2012; Solopova et al., 2014; Sanchez-Romero and Casadesús, 2014). Moreover, recent advances in microfluidics devices delivered a breakthrough in performing long-term time lapse studies of developing cell populations under tightly controlled conditions (Grünberger et al., 2014; Okumus et al., 2014; Rowat et al., 2009; Weaver et al., 2014).

However, simultaneous monitoring of multiple gene activities is hampered by the availability of compatible, non-overlapping fluorescent markers regarding excitation and emission wavelength spectra. To date, studies usually relied on one or two fluorescent markers in a given system. Examples are studies of a bimodal switch controlling biofilm synthesis and sporulation in *Bacillus subtilis* (Chai et al., 2008; Chastanet et al., 2010), bet-hedging strategies in *Lactococcus lactis* (Solopova et al., 2014), variation in quorum sensing (QS) in *Vibrio harveyi*, *Sinorhizobium fredii* NGR234, *Pseudomonas syringae* and *Xanthomonas campestris* (Anetzberger et al., 2012; Grote et al., 2014; Pradhan and Chatterjee, 2014), and antibiotic resistance of subpopulations in *Salmonella enterica* (Sanchez-Romero and Casadesús, 2014). Few studies have successfully implemented three fluorescent markers (Dunlop et al., 2008; Pedraza and van Oudenaarden, 2005).

In this study, we constructed a triple-fluorescent reporter gene cassette applicable to simultaneously monitor activities of three promoters, either integrated into the genome or a plasmid vector. Here, we report on the properties of this triple promoter probe construct and demonstrate its performance by characterizing variations in the expression of representative exopolysaccharide biosynthesis and QS genes in populations of the Gram-negative α-proteobacterium *Sinorhizobium meliloti*. Both processes are candidates for non-uniform phenotypes. Exopolysaccharides (EPS) secreted by this nitrogen-fixing plant-symbiotic bacterium (Jones et al., 2007) represent common goods that serve multiple roles in enhancing survival of the population. EPS support motility and symbiosis, as well as biofilm formation and protection against predators competitors, or harsh physical conditions (Bahlawane et al., 2008b; Lehman and Long, 2013; Pérez et al., 2014; Rinaudi et al., 2010). QS using *N*-acyl homoserine lactones (AHLs) as signal molecules is a widespread mechanism in cell-cell communication that allows bacteria to coordinate their gene expression in response to local population density (González and Marketon, 2003; Von Bodman et al., 2008). Among other processes AHL-dependent regulation controls EPS production in *S. meliloti* (Charoenpanich et al., 2013; Glenn et al., 2007; McIntosh et al., 2008; Pellock et al., 2002). We developed a novel mathematical method for classification of cell types in bacterial populations based on the increase in reporter fluorescence per generation. With regard to production of the EPS galactoglucan in *S. meliloti* colonies, three subpopulations were determined: strong-contributors, weak-contributors, and non-contributors.

2. Materials and methods

2.1. Strains

Strains and plasmids are described in Table 1 and oligonucleotide primers used for genetic constructions are listed in Table S1. Primers for amplification of native *S. meliloti* sequences were designed based on the *S. meliloti* 1021 genome sequence (Galibert et al., 2001).

2.1.1. Construction of fluorophore encoding plasmids

Each of six fluorophore coding genes was first amplified using primer pair Universal-Fluorophore primer-XbaI-fwd and Universal-Fluorophore primer-HindIII-rev. Fragments were each cloned into pSRK_Gm downstream of a tandem arrangement of the isopropyl-β-D-thiogalactopyranoside (IPTG) inducible lac promoter (Plac) and the IPTG inducible T5 promoter (PT5) (derived from pQE-9 vector; Qiagen, Germany) to drive strong expression of the fluorophore genes. The latter was inserted downstream of Plac using primers PT5-NdeI-fwd/PT5-XbaI-rev and NdeI/XbaI restriction sites. The resulting plasmids (pWBT5 series) were introduced to *S. meliloti* strain Sm2B3001 (Bahlawane et al., 2008b) by *Escherichia coli* S17-1 mediated conjugation (Simon et al., 1983) to give strains Sm2B3001-T5^{EBFP2}, -T5^{cerulean}, -T5^{EGFP}, -T5^{mVenus}, -T5^{YPET} and -T5^{mCherry}.

2.1.2. Construction of the triple reporter construct

The triple reporter construct was basically cloned in six consecutive steps. (1) The T5 promoter sequence (derived from pQE-9) was amplified using primer pair PT5-XbaI-fwd/PT5-SpHI-PstI-rev and inserted into the multiple cloning site (MCS I) of pK18mob2_Km (Tauch et al., 1998) using XbaI and PstI restriction sites. (2) The *mCherry* coding region (Shaner et al., 2004) was amplified with mCherry-RBS-PstI-fwd/mCherry-HindIII-rev primers and this fragment was inserted downstream of the T5 promoter into the PstI and HindIII restriction sites. The forward primer carries an artificial RBS sequence. (3) Two synthetic, single stranded DNA fragments, namely MCS II-disrupted-HindIII-fwd and MCS II-HindIII-rev (Table S1), were annealed giving rise to a DNA fragment with HindIII-type overhangs on both sites. This DNA fragment includes MCS II and was inserted downstream of the *mCherry* coding region using HindIII restriction sites. It has to be noted that a single nucleotide relevant for restriction enzyme recognition next to the HindIII overhang (derived from MCS II-disrupted-HindIII-fwd) was exchanged (A/AGCT**T** -> A/AGCT**G**). With this modification multiple occurrences of HindIII sites in MCS-II were avoided. (4) The new inserted MCS II was further used to add an array of four *rrnB* T1 terminator sequences, two in each direction (Ham et al., 2006). After amplification using T1-TTTT-AatII-XbaI-rev/T1-TTTT-SacI-fwd primers the T1 terminator fragment was inserted into MCS II (XbaI\SacI). (5) The amplified *mVenus* coding region (Nagai et al., 2002) (primer pair: mVenus-SalI-fwd/mVenus-HindIII-rev) was cloned into MCS II using SalI and HindIII restriction sites. (6) The amplified *cerulean* coding region (Rizzo et al., 2004) (primer pair: cerulean-EcoRI-rev/cerulean-KpnI-fwd) was inserted into MCS I using EcoRI and KpnI restriction sites. The DNA sequence of the resulting TriFluoR construct is available under GenBank accession no. KP666136.

2.1.3. Construction of the wgeA and sinI promoter probe constructs

Strains Sm2B3001$_{\Delta exoB}$ P*wgeA*^{cer}/P*T5*^{mChe}/P*sin*^{mVen} and Sm2B3001$_{\Delta exoB}$ P*wgeA*^{cer}/P*T5*^{mChe}/P*wgeA*^{mVen} were designed as follows: Promoter fragments were amplified by PCR using Sm2B3001 DNA as template (Bahlawane et al., 2008b) and either primer pair P*wgeA*-BamH1/XbaI-MCS I-fwd and *PwgeA*-KpnI-MCS I-rev (P*wgeA* fragment, 850 bp) or P*sinI*-NdeI-NotI-AatII-MCS II-fwd and P*sinI*-ATG-SpeI-SalI-MCS II-rev (P*sinI* fragment, 305 bp). P*wgeA* and P*sinI* DNA fragments were cloned into MCS I (XbaI/KpnI) and MCS II (AatII/SpeI) of the triple reporter construct, respectively. For Sm2B3001$_{\Delta exoB}$ P*wgeA*^{cer}/P*T5*^{mChe}/P*wgeA*^{mVen} a second P*wgeA* fragment (357 bp) was amplified using primer pair P*wgeA*-SalI-MCS II-rev and P*wgeA*-NdeI-MCS II-fwd. Applying SalI and NdeI

Table 1
Strains and plasmids.

Strains and plasmids	Description	References
Sinorhizobium meliloti		
Sm2B3001	Rm2011 (Casse et al., 1979) with a restored *expR* gene	Bahlawane et al. (2008b)
Sm2B3001$_{\Delta exoB}$	Sm2B3001 with deletion of the *exoB* gene (Δ*exoB*)	Charoenpanich et al. (2014)
Escherichia coli		
E. coli DH5α	For plasmid construction	Grant et al. (1990)
E. coli S17-1	Used for conjugation with *S. meliloti*	Simon et al. (1983)
Plasmids		
pSRK_Gm	pBBR1MCS-5 (Kovach et al., 1995)-derived broad-host-range expression vector containing *lac* promoter and *lacIq*, *lacZα+*, and *aacC1* mediating Gm resistance	Khan et al. (2008)
pWBT5^{EBFP2}	pSRK-derived broad-host-range expression vector containing T5 promoter, artificial RBS and the *ebfp2* gene	This work
pWBT5^{cerulean}	pSRK-derived broad-host-range expression vector containing T5 promoter, artificial RBS and the *cerulean* gene	This work
pWBT5^{mVenus}	pSRK-derived broad-host-range expression vector containing T5 promoter, artificial RBS and the *mVenus* gene	This work
pWBT5^{mCherry}	pSRK-derived broad-host-range expression vector containing T5 promoter, artificial RBS and the *mCherry* gene	This work
pWBT5^{YPET}	pSRK-derived broad-host-range expression vector containing T5 promoter, artificial RBS and the *ypet* gene	This work
pWBT5^{EGFP}	pSRK-derived broad-host-range expression vector containing T5 promoter, artificial RBS and the *egfp* gene	This work
pK18mob2_Km	Suicide vector; *mob lacZ* Km^r	Tauch et al. (1998)
pK18mob2-TriFluoR	pK18mob2_Km carrying triple reporter construct with MCS I-*cerulean*, PT5-*mCherry*, MCS II-*mVenus*	This work
pK18mob2-P*wgeA*^{cer}/PT5^{mChe}/P*wgeA*^{mVen}	pK18mob2_Km carrying triple reporter construct with P*wgeA*-*cerulean*, PT5-*mCherry*, P*wgeA*-*mVenus*	This work
pK18mob2-P*wgeA*^{cer}/PT5^{mChe}/P*sinI*^{mVen}	pK18mob2_Km carrying triple reporter construct with P*wgeA*-*cerulean*, PT5-*mCherry*, P*wgeA*-*mVenus*	This work

restriction sites this fragment was cloned into the former construct via exchange with the P*sinI* fragment.

pK18mob2_Km (Tauch et al., 1998) carrying either the P*wgeA*^{cer}/PT5^{mChe}/P*sin*^{mVen} or the P*wgeA*^{cer}/PT5^{mChe}/P*wgeA*^{mVen} construct were transferred into Sm2B3001$_{\Delta exoB}$ (Charoenpanich et al., 2014) by *E. coli* strain S17-1-mediated conjugation (Simon et al., 1983). Single homologous recombination occurred at the P*wgeA* fragment inserted into MCS I.

2.2. Characterization of fluorophores in S. meliloti

S. meliloti strains carrying pWBT5 with either -T5^{EBFP2} (PT5-RBS-*EBFP2*), -T5^{cerulean} (PT5-RBS-*cerulean*), -T5^{EGFP} (PT5-RBS-*EGFP*), -T5^{mVenus} (PT5-RBS-*mVenus*), -T5^{YPET} (PT5-RBS-*YPET*) or -T5^{mCherry} (PT5-RBS-*mCherry*) were cultivated in MOPS minimal medium containing 0.1 mM phosphate (Zhan et al., 1991) and 10 μg/ml of Gentamycin at 30 °C. Pre-cultures were grown in 96-well microplates with continuous agitation (1200 rpm) for 12 h. Subsequently, cultures were diluted to OD_{600nm} of 0.0001 in a final volume of 100 μl medium additionally supplemented with 0.5 mM IPTG and grown in 96-well microplates for 24 to 48 h with continuous shaking (1200 rpm). Measurements of OD_{600nm} and fluorescence were performed three times per well at different time points applying the Infinite M200 microplate reader (Tecan). The fluorescence of each reporter strain was measured applying the following excitation (Ex) and emission (Em) settings: EBFP2 (Ex 383 nm, Em 448 nm), cerulean (Ex 447 nm, Em 483 nm), mVenus (Ex 515 nm, Em 548 nm), YPet (Ex 515 nm, Em 548 nm), EGFP (Ex 488 nm, Em 522 nm) and mCherry (Ex 585 nm, Em 619 nm).

2.3. Microfluidics

Bacterial growth and reporter gene activities were monitored in the B04A Microfluidic Bacteria Plate (Cellasic) (EMD Millipore Corporation, 2014). After removing the plate from the vacuum package, the PBS-Buffer was removed from all wells. Subsequently, to remove any PBS residuals, each well was washed with 200 μl MOPS minimal medium (2 mM phosphate). In the next step 100 μl medium was added to all wells except the waste collection well, and the pre-filled microfluidic plate was connected to the manifold of the Cellasic ONIX Microfluidic Platform (EMD Millipore Corporation, 2014). After initiation of the ONIX FG software the "Pre-loading" protocol was used (Table S2). Pressure (4 psi) was initially applied to all wells containing media for 5 min. In a second step maximum pressure (8 psi) was applied to all columns for 2 min to expand the cavities.

Pre-cultures of different *S. meliloti* strains were grown to OD_{600nm} of ~0.1 (logarithmic phase) in MOPS minimal medium containing 2 mM phosphate (Zhan et al., 1991). Prior to injection into the Cellasic cavity system the cells were highly diluted in pre-warmed MOPS minimal medium (2 mM phosphate) to OD_{600nm} of ~0.0005. According to the user's manual 50 μl of the diluted cell suspension and 300 μl MOPS minimal medium (2 mM phosphate) were pipetted into the cell loading and the medium reservoir well, respectively. The plate was reconnected to the manifold and the "Load" protocol was initiated (Table S2). Here the cells were loaded into the microfluidic trap followed by a gentle washing step to remove loosely trapped bacteria. Finally, a constant medium flow (0.25 psi) provided a constant nutrient supply for all trapped bacteria.

2.4. Long-term time lapse microscopy

Long-term observation of trapped bacteria was performed using the Eclipse Ti-E inverse research microscope (Nikon) in an incubation chamber which assured a constant temperature of 30 °C. Selection of appropriate individuals for observation and determination of their spatial *x* and *y* coordinates was carried out using the live imaging modus provided by the NIS elements software (Nikon). Phase contrast and fluorescence pictures of each selected individual/colony were taken automatically each 30 min with the IXON X3885 camera (Andor, Oxford Instruments). For fluorescence

microscopy two laser sources – a green DPSS solid state laser (561 nm, 50 mW) (Sapphire) and a multiline Argonlaser (65 mW) (Melles Griot) – were applied. For fluorophore excitation and emission detection, specific interference and absorption filter sets were applied for cerulean (Rizzo et al., 2004), mCherry (Shaner et al., 2004), and mVenus (Nagai et al., 2002). Each filter set consists of an excitation filter (EXF), a dichromatic mirror (DM), and a barrier (or emission) filter (BAF). Features of the applied filter sets: (i) mCherry: EXF: 562/40 nm, DM: 593 nm, BA: 624/40 nm bandpass; (ii) mVenus: EX: 500/24 nm, DM: 520 nm, BA: 542/27 nm bandpass; (iii) cerulean: EX: 438/24 nm, DM: 458 nm, BA: 483/32 nm bandpass. To reduce background fluorescence the highly inclined laminated optical sheet (HILO) technique was applied (Tokunaga et al., 2008). For each channel appropriate exposure times, multiplier values and conversion gains were selected to assure constant and optimal illumination.

2.5. Data processing

Image processing, binary layer construction, segmentation and raw data acquisition was performed using the NIS-Elements software (Nikon). For each colony in each frame the background fluorescence of each marker was measured at four independent locations. For every single measurement time the mean of the background fluorescence was then subtracted from the measured fluorescence values (Tables S3 and S4). From this modified data we calculated the mean (Table S5). As a measure of dispersion we computed the coefficient of variation, i.e. square root of the variance divided by the mean. For determining the correlations between the markers we normalized the fluorescence data at each measured time by dividing the values by their mean.

In order to compare the colonies with each other we unified the fluorescence values. Therefore, we first chose a reference colony. Next, we multiplied all fluorescence values with the corresponding mean of the reference colony at every single time point and divided it by their own mean (Table S4). These transformed data were used for the classification (Table S6) (see below). As before, the dispersion was measured by the coefficient of variation whereas the correlations between the fluorescence markers were calculated with the normalized data (division by mean).

2.6. Classification of cell types

For the classification of the cells we used the mVenus fluorescence data. We considered complete fluorescence profiles rather than single fluorescence values. Since gene expression can be represented by a gamma distribution (Lipniacki et al., 2006; Müller et al., 2008) the rate and the shape parameter for the different cell states have to be estimated.

2.6.1. Estimation of parameters of gamma distributions

In the first step three cells for each class, non-contributor (NC), weak contributor (WC), strong contributor (SC), which displayed the defined characteristic behavior were chosen. The fluorescence data of the selected reference cells are shown in Fig. S1. For the NC-class we performed a maximum likelihood estimation for the two parameters of a gamma distribution on the increase between two measurements. We assumed that increases between the time steps are independent. For the WC-class we took the data starting from the time when there was a first increase of at least 15 FU (fluorescence units) between two measurements (32 min) which is approximately the mean increase value in a cell cycle (approximately 3 h) for the cells chosen for estimation. Concerning the SC-class we followed the same approach as for the WC-class with two differences. First, we increased the threshold to 32 FU (again about the mean fluorescence increase in 30 min). Second, we used the increase in fluorescence values only until a certain fluorescence intensity is reached. This fluorescence threshold was set to 500 FU since above this value some cells showed an accumulative behavior in fluorescence. This procedure provides the estimated shape and rate parameters $\widehat{p_J}$ and $\widehat{b_J}$, respectively, for $J \in \{\mathrm{NC}, \mathrm{WC}, \mathrm{SC}\}$.

2.6.2. Classification

One possibility is classification according to the increase in gene expression, but as revealed in Fig. S2a the three types are not easily distinguishable within 30 min time frames. Therefore, we looked at the increase of fluorescence per generation time (FIPG) which is about 3 h (Fig. S2b). In order to do so we first estimated the mean generation time of the data, denoted by $\hat{g}$ and considered the variables

$$T_J := \sum_{i=1}^{g} S_i^J \sim \gamma\left(gp_J,\, b_J\right),$$

which describe the FIPG. Here, S_i^J are random variables representing the 30 min increase of type J and p_J and b_J are the shape and rate parameter of the gamma distribution of type J. Implicitly, we assume that the cell type is fixed within the life cycle of a cell. This is reasonable since switches from the NC to the WC or SC state are irreversible, at least in a short period of time. By studying the random variables T_J instead of S_i^J the three types can be distinguished more easily (compare Figs. S2a and b for S_i^J and T_J, respectively). Furthermore, small temporal fluctuations in gene expression have no influence on the classification under T_J.

The classification was performed by calculating the likelihood value for the maximal FIPG along the ancestral lineages of a cell for each of the three distributions belonging to the three classes and assigning each cell to the class with the highest likelihood value. This classification has two specificities: first, the maximum has a different distribution as the increase in a single generation time and second, fluorescence increases between cells are correlated due to common ancestry. The first issue is only relevant for the NC-class. Here, the maximal FIPG is larger than the increase between two cell divisions. However, this has only a moderate effect on the classification of NCs (less than 20% of the cells), see Fig. S3a. For the WC-class this problem is not visible when looking at the density (Fig. S3b) nor is it for the SC-class (Fig. S3c). As to the inaccuracy introduced by the correlation of the maximal FIPG due to common ancestry, here this is not relevant since the maximal FIPG typically occurs after at least four life cycles. Thus, each maximal FIPG only affects a small fraction of the population.

3. Results

3.1. Composition and features of the triple fluorescent reporter cassette

To construct the triple promoter probe cassette (Fig. 1), three compatible fluorescent markers with appropriate excitation (Ex) and emission (Em) wavelengths were selected from a set of six fluorophores.

3.1.1. Selection of compatible fluorescent markers

The six fluorescent proteins EBFP2, cerulean, EGFP, mVenus, YPET, and mCherry, were characterized for activity and interference of Ex and Em spectra in *S. meliloti*. Detailed information about each fluorophore is given in Fig. S4a. Fluorophore output signals of *S. meliloti* strains Sm2B3001-T5$^{\mathrm{EBFP2}}$, -T5$^{\mathrm{cerulean}}$, -T5$^{\mathrm{EGFP}}$, -T5$^{\mathrm{mVenus}}$, -T5$^{\mathrm{YPET}}$ and -T5$^{\mathrm{mCherry}}$ each expressing a plasmid-borne copy of one of the six different fluorophore genes were determined.

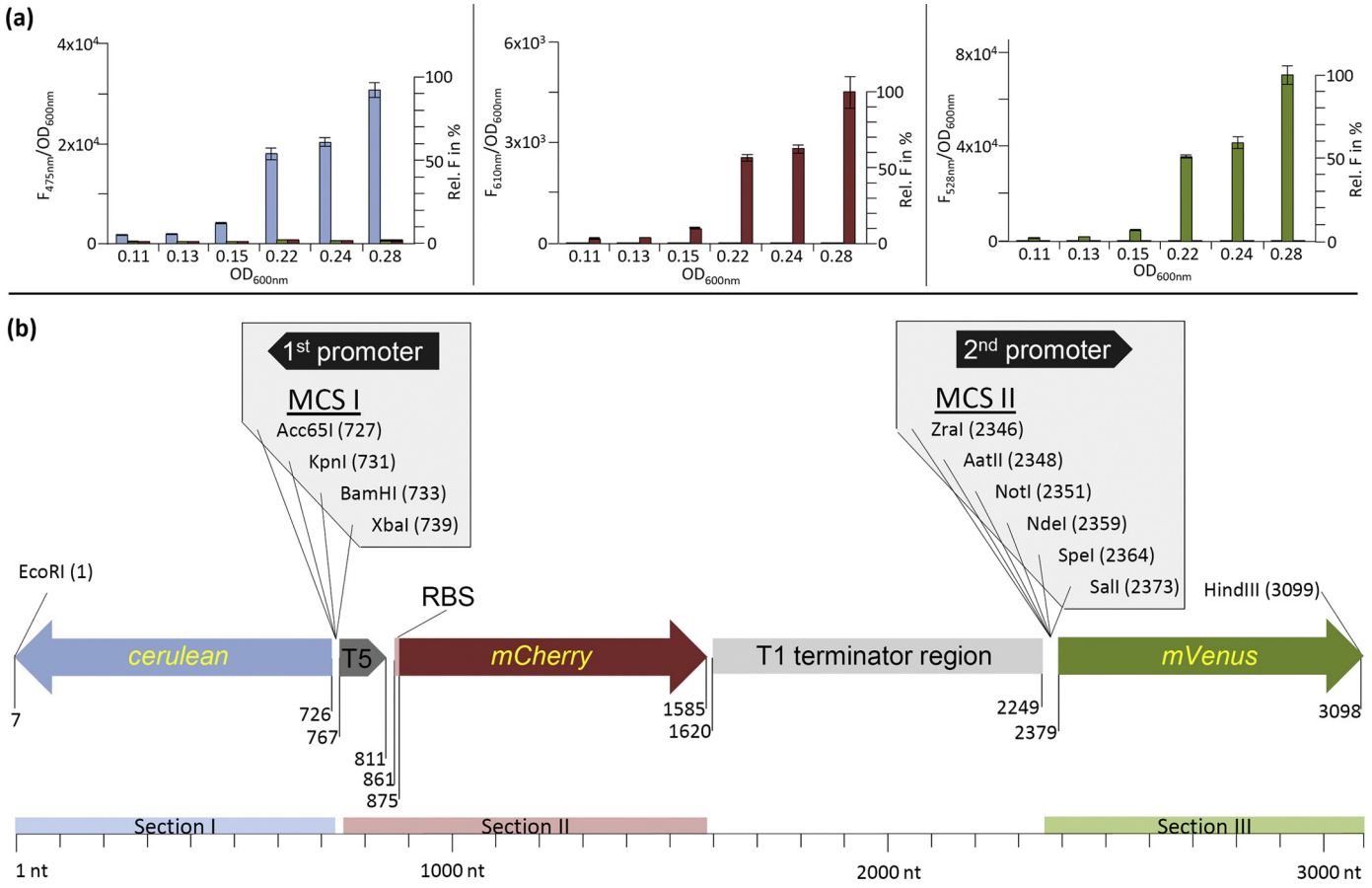

Fig. 1. (a) Fluorescence profiles conferred by *cerulean*, *mCherry* and *mVenus* expressed from plasmid pWBT5. The emission profile of each fluorophore was monitored applying EX and Em parameters of cerulean, mCherry and mVenus. *Y*-axis (left), fluorescence per OD_{600nm}; *Y*-axis (right), relative fluorescence in %; *X*-axis, OD_{600nm}. (b) Triple fluorescent reporter (TriFluoR) promoter probe construct. The construct includes the three fluorescent marker genes *cerulean*, *mCherry* and *mVenus* (blue, red and green colored arrows, respectively), multiple cloning sites I and II (light gray boxes with restriction sites), a single T5-promoter (dark gray arrow) with artificial RBS (light red) and a region that includes four *E. coli* T1 terminator motifs (gray box). Construct size in nucleotides (nt) is denoted by the scale below.

Fluorescence signals of each reporter strain were monitored during culture growth according to previously defined combinations of Em and Ex wavelengths (Fig. S4b). Note, that Ex and Em parameters for YPET and EGFP are the same (Fig. S4b).

As expected, each fluorescent reporter produced significant emission signals at the defined Ex wavelength (Fig. S4b and Fig. 1a). Cerulean and mCherry only emitted detectable signals when excited by their defined Ex wavelength. However, applying mVenus, EGFP, and EBFP Ex wavelengths and their corresponding detection parameters, different degrees of emission "cross-contamination" were observed for these reporters (Fig. S4b). In summary, the results clearly suggest the cerulean, mVenus and mCherry fluorophores as appropriate set for construction of the triple reporter construct (Fig. S4b and Fig. 1a).

Fluorophore specific features including brightness, photo stability, protein folding/degradation rates, and association/dissociation rates when forming active multimers may influence and modulate the emission profile of each fluorescent marker to an unknown degree. Since the three selected fluorophores occur as active monomers, effects of different association and dissociation rates can be disregarded. When expression of the plasmid-borne fluorophore genes was driven by the induced lac and T5 promoters the fluorescence/$OD_{600\,nm}$ ratios of the three selected fluorophores generally increased over time, but each to a different degree (Fig. 1a). Nonetheless, comparing the relative increase over time (maximum values set as 100%) a clear correlation in signal accumulation of cerulean, mCherry and mVenus was observed implying similar properties in biosynthesis and degradation despite a difference in fluorescence intensity.

3.1.2. *Features of the triple fluorescent reporter cassette*

The ~3.1 kb cassette, referred to in this study as the TriFluoR construct, consists of three functional units (Fig. 1b). Section 1 contains the *cerulean* coding region preceded by multiple cloning site I (MCS I). This MCS comprises several restriction sites for integration of the first promoter region of interest (1st promoter) including its native RBS and the start codon of the downstream gene to become the translational start of the reporter gene.

The second unit is oriented in opposite direction to the first section and includes the *mCherry* coding region. This reporter was placed under the control of the T5 promoter followed by an artificial RBS to include a control that can serve as normalization signal.

The third section includes a second MCS (MCS II) followed by the *mVenus* coding region. MCS II offers six restriction sites for insertion of a second promoter region of interest followed by its native RBS and start codon (2nd promoter). Both the *mCherry* and *mVenus* section are located in the same orientation. Consequently, to avoid read-through of the T5 promoter into the downstream *mVenus* coding region four copies of the *E. coli rrnB* terminator T1 were incorporated between both sections. The TriFluoR construct is flanked by two unique restriction sites (EcoRI and HindIII) which facilitate its insertion into other plasmid backbones and thereby its application in other bacteria.

3.2. A test case: Monitoring activity of a galactoglucan biosynthesis gene promoter

EPS biosynthesis places a heavy metabolic burden on individuals when nutrients are scarce. It is therefore tempting to speculate that not all individuals of a population engage in EPS production making EPS biosynthesis genes ideal candidates for heterogeneous expression. In *S. meliloti* colonies, a resolvase-based in vivo expression technology (RIVET) assay provided first hints to heterogeneous expression of *wggR* (Gao et al., 2012) encoding a transcriptional activator of galactoglucan biosynthesis (Bartels et al., 2003; Baumgarth et al., 2005). The 32 kb galactoglucan biosynthesis gene cluster is composed of five operons, with the *wga* and *wge* operons comprising the majority of the biosynthetic genes (Bahlawane et al., 2008a; Becker et al., 1997). Here, we employed the Tri-FluoR promoter probe cassette to characterize the activity of the *wgeA* promoter driving transcription of the *wge* operon. Cells were monitored in a microfluidics setup to study promoter activity in a growing colony under controlled environmental conditions.

The triple reporter cassette enables simultaneous monitoring of the activity of the well-characterized constitutive T5 control promoter and two test promoters. To confirm that *cerulean* and *mVenus* can serve as reporter genes in comparative studies of two test promoters a validation experiment was designed in which both fluorescent marker genes were controlled by the same promoter. To this end, two copies of the *wgeA* promoter were inserted into the reporter cassette upstream of the *cerulean* and the *mVenus* coding regions. The pK18mob2 plasmid carrying the P*wgeA*^{cer}/PT5^{mChe}/P*wgeA*^{mVen} reporter construct was integrated into the genome of the non-EPS producing mutant strain Sm2B3001$_{\Delta exoB}$ by homologous recombination at P*wgeA*^{cer}. Due to deletion of *exoB*, controlling an early step in EPS precursor biosynthesis, galactoglucan production is interrupted without significantly affecting expression of galactoglucan biosynthesis genes or viability (Buendia et al., 1991; Charoenpanich et al., 2014). In the validation experiment, a non-EPS producing strain was employed to avoid interference from copious EPS secretion, which affects supply of nutrients and image acquisition in the microfluidics setup. This strain and the parent Δ*exoB* mutant showed a similar growth behavior in batch cultures (data not shown) indicating that expression of the three fluorescence reporter genes did not negatively affect the generation time.

After loading and trapping of Sm$_{\Delta exoB}$ P*wgeA*^{cer}/P*T5*^{mChe}/P*wgeA*^{mVen} cells in the microfluidic cavities, appropriate individuals for observation were selected aiming at maximizing the distance between neighboring colonies to minimize inter-colony interactions. Colony development was monitored over ~21 h taking frames every 30 min in phase contrast (PH) and three fluorescence detection modes: cerulean (cer), mVenus (mVen) and mCherry (mChe). In total, 10 independent colonies were observed (Table S5). The average doubling time of 2.2 h (determined for the 1 to 10 h period) increased to 3.3 h in the second half of colony development (11 to 21 h) (Table S5). As exemplified by colony 6, all Sm2B3001$_{\Delta exoB}$ P*wgeA*^{cer}/P*T5*^{mChe}/P*wgeA*^{mVen} individuals showed typical colony development starting with a single cell growing into a population of hundreds of cells (Table S5, Fig. 2a). After 5 h the first cell divisions yielded a small cluster of 3 to 9 bacteria (Table S5). During this time overall fluorescence activities decreased. The mean of transformed intensity units (all colonies) conferred by mCherry, mVenus and cerulean shifted from 1576 to 1196 FU, 1798 to 448 FU, and 1292 to 416 FU, respectively. Although this pattern applies to each monitored colony, some variation of average fluorescence between the colonies was observed (Table S5). Possible explanations for this variation are different states of the pre-cultured colony-founding cells and slight variations in environmental conditions at different locations in the microfluidic cavities.

After 10 h the number of individuals per colony ranged from 15 to 33 and the average fluorescence of all colonies further decreased to 1026 FU (PT5^{mChe}), 117 FU (P*wgeA*^{mVen}), and 182 FU (P*wgeA*^{cer}) (Table S5). These values represent the mean minima for virtually all fluorophores within the whole observation period (P*wgeA*^{mVen} activity only slightly decreased further until 15 h (117–98 FU)). We applied these minima values to identify individuals which show strong variations in their fluorescence pattern (each threshold is set as 3 × minimum). E.g., for the 10 h time point two individuals in colony 6 were identified which show a strong re-increase of P*wgeA*^{mVen} fluorescence (Table S5). After 15 h colonies comprised 59–114 individuals and 0 to 41 cells exhibited an increase in P*wgeA*^{mVen} fluorescence. Six hours later several hundred individuals (203–345) formed the mature colonies each with a distinct proportion of cells (26–240) with significantly changed P*wgeA*^{cer} and P*wgeA*^{mVen} activity profiles (Table S5).

The overall activity of T5^{mChe} decreased in the first 10 h and afterwards continuously increased (Table S5). Considering all colonies, only two individuals (in colony 6) showed significant deviation from the threshold in the T5^{mChe} channel (Table S5). This activity profile suggests T5 as constitutive and homogeneous promoter in *S. meliloti*. The high fluorescence at the beginning and the decrease in fluorescence in the first hours of observation may be explained by the abrupt change of growth conditions when precultures (OD_{600} ~0.1) were highly diluted (OD_{600} = 0.000008) for injection into the microfluidic chambers.

PwgeA^{cer} and PwgeA^{mVen} activity patterns show strong correlation. Correlation values between activities of P*wgeA*^{cer} *and* P*wgeA*^{mVen} were determined for all colonies at the 10 h (269 individuals), 15 h (941 individuals) and 21 h (2883 individuals) time points. Correlation values were calculated for each individual colony separately and additionally for a combined data set of all colonies. A normalization step was performed in which the data points of each colony were normalized by its corresponding mean at each time point (Table S3). A clear case of correlation between these two promoter copies was found. After 10, 15 and 21 h the degree of correlation was about 0.82, 0.89 and 0.91, respectively (Table S6 and Fig. 3a). All observed correlations are highly significant ($p < 10^{-15}$). After 21 h, the highest correlation of 0.98 was observed for colony 7 while the lowest value, 0.85, was deduced from colony 4 (Table S6). Lower correlation values in single cells may have been caused by multiple sources of noise including intrinsic noise, such as the stochastic nature of polymerase-promoter interactions (Elowitz et al., 2002), but also slight variations in fluorophore maturation, stability and detection.

In addition, we calculated the correlation values of both P*wgeA* controlled reporters each compared to the PT5^{mChe} signal. As expected, the degree of correlation between P*wgeA* and PT5 was considerably lower. In case of P*wgeA*^{mVen}/PT5^{mChe}, correlations of 0.33, 0.14 and 0.02 were observed after 10, 15 and 21 h, respectively (Table S6). The high degree of correlation between fluorescence signals mediated by P*wgeA*^{cer} and P*wgeA*^{mVen} imply that multiple copies of this promoter behave similarly within a single cell. Furthermore, the high correlation promotes confidence in the applicability of the reporter cassette for comparative promoter studies.

3.3. PwgeA^{cer} and PsinI^{mVen} activity patterns do not correlate

S. meliloti strain Sm2B3001 possesses the Sin QS system composed of the AHL synthase SinI and the two LuxR-type transcription regulators SinR and ExpR. AHLs synthesized by SinI activate ExpR and regulate transcription of a large number of target genes including the galactoglucan biosynthesis genes and *sinI*. The latter

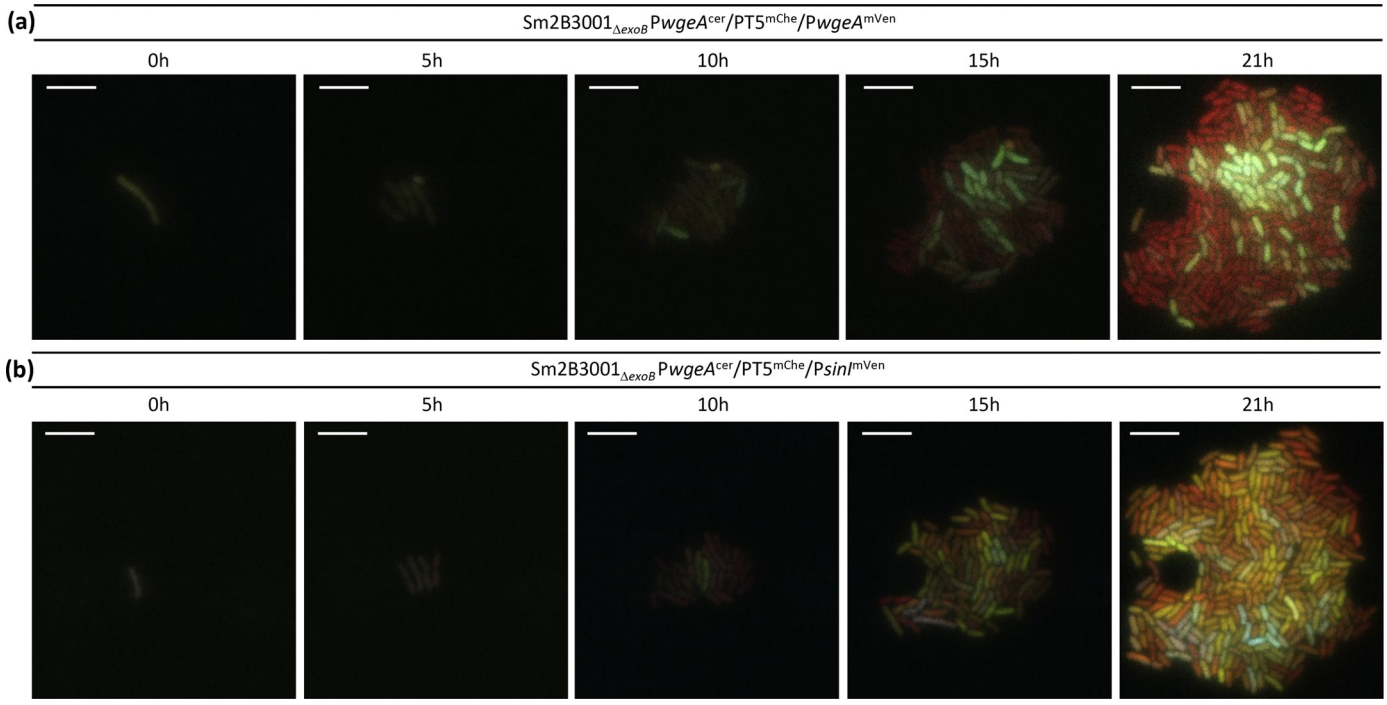

Fig. 2. Colony 7 and Colony 4 of Sm2B3001$_{\Delta exoB}$ P*wgeA*^{cer}/PT5^{mChe}/P*wgeA*^{mVen} and Sm2B3001$_{\Delta exoB}$ P*wgeA*^{cer}/PT5^{mChe}/P*sinI*^{mVen}, respectively. Each colony was observed for 21 h in intervals of 30 min. Representative images taken after 0, 5, 10, 15 and 21 h are shown. Images represent an overlay of the three applied fluorescent markers (cerulean, mCherry, and mVenus). White bar, 5 μm scale.

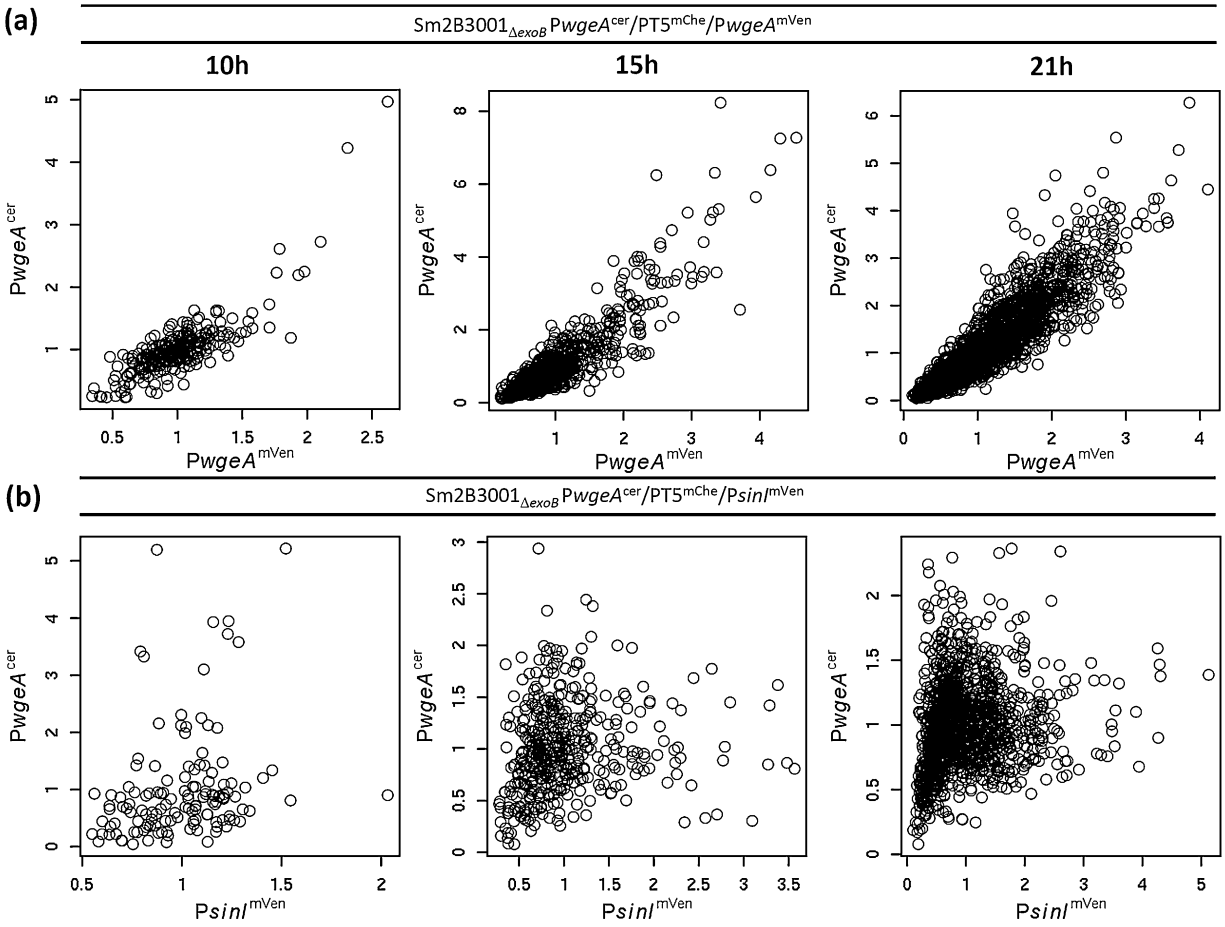

Fig. 3. Correlation between promoter activities. (a) P*wgeA*^{cer}/PT5^{mChe}/P*wgeA*^{mVen}. X- and Y-axis corresponds to normalized P*wgeA*^{mVen} and P*wgeA*^{cer} fluorescence values, respectively. (b) P*wgeA*^{cer}/PT5^{mChe}/P*sinI*^{mVen}. *X*- and *Y*-axis corresponds to normalized P*sinI*^{mVen} and P*wgeA*^{cer} fluorescence values, respectively.

results in positive feedback regulation (Charoenpanich et al., 2013; McIntosh et al., 2009). Activity patterns of the *sinI* and *wgeA* promoters in individual cells were compared by time lapse studies in the microfluidics setup to elucidate if this regulatory link results in correlation of QS and galactoglucan biosynthesis gene expression.

1273 individuals of five independent Sm2B3001$_{\Delta exoB}$P*wgeA*^{cer}/PT5^{mChe}/P*sinI*^{mVen} colonies, each grown from a single cell in the microfluidics chamber, were analyzed. Within the observation periods of 1 to 10 and 10 to 21 h the doubling time (2.3 h and 3.4 h) was comparable to that of the previously analysed Sm2B3001$_{\Delta exoB}$P*wgeA*^{cer}/PT5^{mChe}/P*wgeA*^{mVen} colonies (2.2 h and 3.2 h) (Table S5). As exemplified by colony 4, P*sinI*^{mVen} activity patterns strongly differed from that of P*wgeA*^{cer}. Comparing the activity profile of P*wgeA*^{cer} to the profile produced by P*wgeA*^{cer} in the previous experiment we observed a similar behavior (Fig. S5), indicating high correlation in expression behavior between independent colonies.

Interestingly, P*sinI* activity generally emerged 3 h earlier than that of P*wgeA*^{cer} (Table S5). Furthermore, the activation of P*sinI* was observed in almost every individual at later time points, i.e. after 15 and 21 h. This behavior is completely different to that of P*wgeA* where differences in fluorescence intensity between individuals was larger and persisted until the last measurement (21 h). To address the question if P*wgeA* activation correlates with P*sinI* activity in individual cells, the degree of correlation between P*wgeA*^{cer} and P*sinI*^{mVen} activities was calculated for the 5 colonies. This revealed low correlation values of 0.26, 0.15 and 0.17 after 10, 15 and 21 h, respectively (Table S6, Fig. 3b).

3.4. Variance patterns demonstrate heterogeneous PwgeA activity

All analyzed colonies consist of two broad classes of individuals which can either be described by an active or by a non-active *wgeA* promoter. Thus, we addressed the questions of whether the activity of P*wgeA* can be classified as heterogeneous or homogeneous and how the behavior of P*wgeA* compares to that of PT5 and P*sinI*. We hypothesize that homogeneous and heterogeneous promoter elements can be characterized via calculation of their coefficient of variation (variance divided by mean) values. Generally, variance is the spreading of data around their mean. For promoter activity it means the higher the variance the less homogeneous is the promoter behavior. First, the already modified data sets of the ten Sm2B3001$_{\Delta exoB}$P*wgeA*^{cer}/PT5^{mChe}/P*wgeA*^{mVen} colonies were applied to generate coefficient of variation values for PT5^{mChe}, P*wgeA*^{cer}, and P*wgeA*^{mVen}.

PT5^{mChe} possesses a low variance over time with variation values of 0.17, 0.18, 0.23 and 0.27 after 5, 10, 15 and 21 h, respectively. As exemplified by the 21 h time point the gamma distribution for the normalized fluorescence intensities is more compact (Fig. 4a). The low variance strongly supports our previous intuitive classification of the PT5 activity as homogeneous.

In contrast, variance of P*wgeA* activity with coefficient of variation values of 0.26, 0.30, 0.6 and 0.6 (cerulean) and 0.19, 0.47, 0.93 and 0.8 (mVenus) were calculated for the 5, 10, 15 and 21 h time points, respectively (Fig. 4a and Table S6). The results showed that variance significantly increased during the observation period. As displayed in Fig. 4a at the 21 h time point promoters with high variance values can also be described by the spread of gamma distributions with elongated tails at the end. Since we hypothesized that a high degree of variance and wide spreading gamma distributions are typical features for heterogeneous promoter elements a clear evidence for heterogeneity of P*wgeA* is given.

Applying the transformed data of five Sm2B3001$_{\Delta exoB}$P*wgeA*^{cer}/PT5^{mChe}/P*sinI*^{mVen} colonies we also calculated the coefficient of variation of P*sinI* activity compared to the corresponding PT5 and P*wgeA* values. P*wgeA* and PT5 meet expectations and were again classified as heterogeneous and homogeneous, correspondingly (Fig. 4b). The promoter of *sinI*, however, shows a different behavior compared to both P*wgeA* and PT5. Starting with a very low variation value of 0.21 after 5 h, the coefficient of the variance strongly increased to 0.94 after 10 h and finally decreased to 0.34 after 21 h, which is only slightly higher than the coefficient of variation of PT5 (Fig. 4b and Table S6). Thus, behavior of P*sinI* and P*wgeA* clearly differ since P*wgeA* variance increased over virtually the whole observation period.

3.5. Definition of contributor and non-contributor classes

We found a clear case of phenotypic heterogeneity in *S. meliloti* populations based on P*wgeA* activity. Since P*wgeA* controls expression of genes relevant to galactoglucan biosynthesis we assume that only subgroups of the observed *S. meliloti* population significantly produced enzymes for galactoglucan production. To clearly define which proportion of individuals contributes and which do not, we were looking for a reasonable indicator allowing a reliable classification of different cell states. We have developed a novel method to determine cell states, which is based on the maximal FIPG. FIPGs reliably describe the degree of fluorophore gene expression even before the final maximum of fluorescence is reached. They allow the classification of distinct cell states within short time periods since the FIPGs can be calculated with data from only a few (at least two) time points.

A closer look at the P*wgeA*^{mVen}-controlled level of fluorescence and cell lineages observed over time (see for example Fig. 5a) broadly suggests three prominent types of lineage curves, all of which are assumed to follow a gamma distribution as explained in materials and methods. We also checked for two types but the fit was not satisfactory, see Fig. S6. The NC (low level of activity), WC (slow but continuous increase) and SC (exponential increase) classes have estimated shape and rate parameters of 0.2, 0.46, 0.64 and 0.06, 0.03, 0.01, respectively. We also checked the dependence of the parameter estimates on the colony, which is negligible since all estimates provide satisfactory approximations (compare orange curve and step function in Fig. S6).

For the actual classification of individuals we applied a more detailed data set of the ten individual Sm2B3001$_{\Delta exoB}$ P*wgeA*^{cer}/PT5^{mChe}/P*wgeA*^{mVen} colonies (Table S4). This data set includes detailed records for each individual once relevant P*wgeA*^{mVen} activity was observed. Since cells without any significant increase in P*wgeA*^{mVen} mediated fluorescence can easily be determined as NC we only selected a representative number of NCs for further analysis. An example of recorded cell lineages is given in Fig. 5a. Performing a principal component analysis with the single step increase, generation increase, mean generation increase and their maximal values over the cell history the maximal FIPG turned out to have the strongest influence on the fluorescence values mediated by P*wgeA*^{mVen}. Using the predefined "princomp" procedure in R we obtain the following weights for the first loading vector: maximal FIPG = 0.965, single step increase = 0.226, maximal mean generation increase = 0.13, the other components have weight 0. Therefore, we took the maximal FIPG of the progeny of each cell and classified according to these values via a gamma mixture model with fixed distribution parameters as explained in materials and methods. Note that we classify only according to increases in fluorescence level, i.e. transitions from lower to higher expression states. Conversions back to cell types displaying lower expression levels remain to be studied.

As shown in Fig. 5b, NCs (black curve) are estimated to possess no or very little FIPG. Slight increases in P*wgeA* activity are in agreement with the low basal activity of P*wgeA*. Weak contributors (blue curve) revealed a moderate FIPG. Most individuals showed

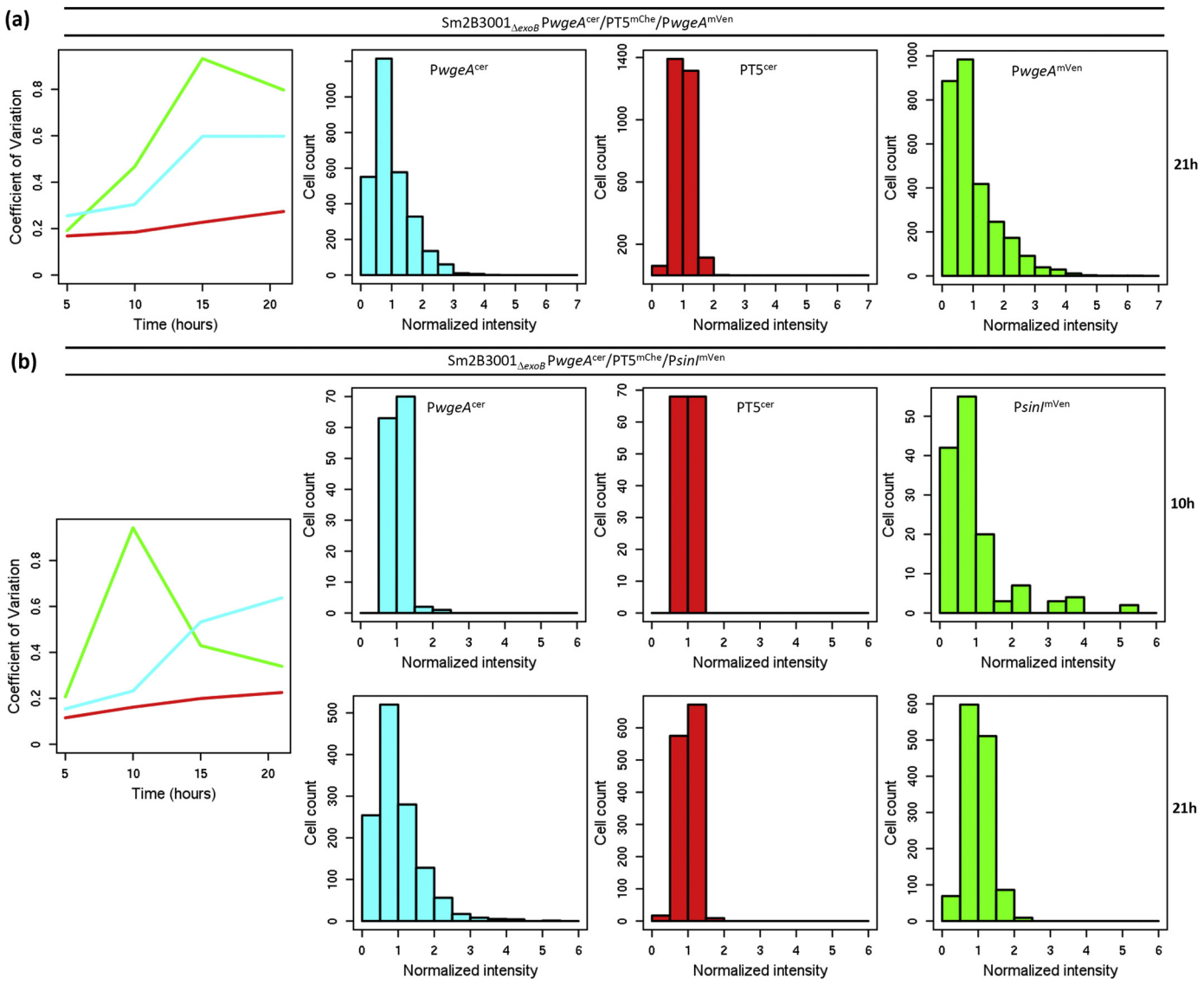

Fig. 4. Variance of P*wgeA*^{cer}, P*wgeA*^{mVen}, PT5^{mChe}, and PsinI^{mVen} activities. (a) Coefficient of variation over time of PT5^{mChe}, P*wgeA*^{cer} and P*wgeA*^{mVen} mediated fluorescence intensity and histograms of normalized fluorescence intensities of P*wgeA*^{mVen}, P*wgeA*^{cer} and PT5^{mChe} at the last measured time point. (b) Coefficient of variation over time of PT5^{mChe}, P*wgeA*^{cer} and P*sinI*^{mVen} mediated fluorescence. Histograms for PT5^{mChe}, P*wgeA*^{cer} and P*sinI*^{mVen} as described in (a) but for an additional time point (10 h).

increases in fluorescence of around 80 to 100 fluorescence units (FU) per generation time. The class of strong contributor cells is estimated to have a mean increase of about 200 FU (green curve). Although these concrete values change when using different reference colonies, the overall pattern of heterogeneity with NC, WC and SC classes remains (Fig. S7).

Applying this novel classification approach, the proportions of the different cell types regarding P*wgeA* activity profiles were calculated. For the whole P*wgeA* data set derived from the dual reporter experiment, the NC, WC and SC classes are represented by 36%, 33% and 31% of the cells (Fig. 5c).

Finally, we determined the average occurrence of cell types for the Sm2B3001$_{\Delta exoB}$ P*wgeA*^{cer}/P*T5*^{mChe}/P*sinI*^{mVen} data set. The average proportions of NC, WC and SC cell types differ only slightly from that of the former analyzed colonies with 24%, 49%, and 27%, respectively (Fig. 5c, Table S6).

However, regarding all 15 colonies from both strains individually we observe a strong fluctuation in cell type proportions (Table S6). Extreme examples are given for colony 2 of strain Sm2B3001$_{\Delta exoB}$ P*wgeA*^{cer}/P*T5*^{mChe}/P*wgeA*^{mVen} and for colony 2 of strain Sm2B3001$_{\Delta exoB}$ P*wgeA*^{cer}/P*T5*^{mChe}/P*sinI*^{mVen} where no SC cells were detected (Table S6).

Since P*sinI* passes only through a short time period of heterogeneous behavior before it finally becomes homogeneous we omit classifying individuals by their corresponding P*sinI* activities.

4. Discussion

Monitoring heterogeneity in gene expression strongly builds on microscopic live cell imaging employing transcriptional or translational fusions to fluorescent reporter genes. A growing number of studies are applying fluorescent marker-based strategies to investigate how and why heterogeneity occurs in bacterial populations. Here, we introduced a new strategy to elucidate heterogeneous gene expression based on the TriFluoR triple promoter probe cassette. Compared to previous studies employing a single (Anetzberger et al., 2012; Chai et al., 2008; Grote et al., 2014; Pradhan and Chatterjee, 2014; Sanchez-Romero and Casadesús, 2014) or two fluorescent reporters (Fagerlund et al., 2014;

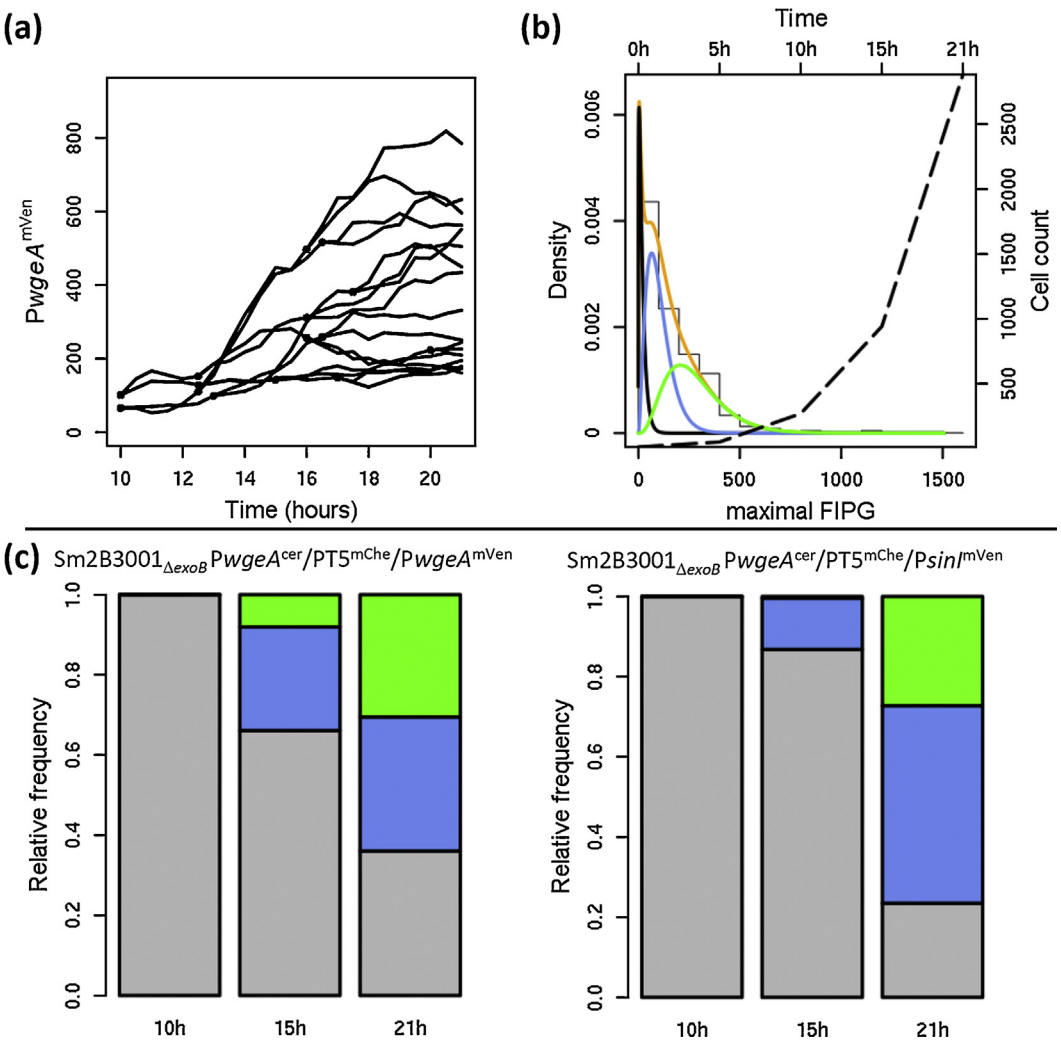

Fig. 5. (a) Fluorescence intensity of a cell (colony 7) and its progeny. (b) Estimated gamma mixture model and cell counts. The plot shows the estimated density for the maximal FIPG (orange) and the corresponding data of all measured colonies (step function). The black, blue and green curves correspond to the separate estimates of the gamma distributions for the NC, WC and SC class, respectively. The dashed line corresponds to the cell counts (right *y*-axis) of all colonies over time (upper *x*-axis). The lower *x*-axis is given by the maximal FIPG whereas the left *y*-axis shows the values of the probability density functions. (c) Classification of different cell states. Relative distribution of NC (gray), WC (blue) and SC (green).

Miao et al., 2009; Solopova et al., 2014) we added a third reporter, and gaining from the growing portfolio of fluorescent proteins employed only monomeric highly compatible fluorescent proteins as reporters. The T5 promoter was fused to one of the three reporter genes to serve as a homogeneously active control, which can be applied for normalization. Moreover, the three promoter probe constructs were joined in a compact versatile cassette.

Our test case validated the performance of this reporter cassette and also provided new insights into heterogeneity of EPS production and QS in isogenic *S. meliloti* populations. EPS functions, biosynthesis pathways, and their regulation have extensively been studied (Bahlawane et al., 2008a,b; Baumgarth et al., 2005; Becker et al., 2002, 1997; Gao et al., 2012; McIntosh et al., 2008). However, little is known about the engagement of individuals of a population in this highly energy-demanding production process. The galactoglucan biosynthesis gene cluster is composed of the *wga* (10 genes), *wgcA* (1 gene), *wggR* (1 gene), *wgd* (2 genes), and *wge* (8 genes) operons (Becker et al., 1997; Rüberg et al., 1999). It has been shown that the expression of these operons is controlled by phosphate limitation and the regulatory genes *mucR* and *expR* and that this expression is essential for the production of this EPS (Rüberg et al., 1999; McIntosh et al., 2008). Since the *wge* operon was most strongly induced in these conditions its promoter was chosen as an indicator for galactoglucan biosynthesis in our study. Here, we clearly demonstrated a heterogeneous activity pattern of this promoter. The observed pattern suggests that, under the conditions tested, only one-third of the individuals in a *S. meliloti* colony strongly invest in galactoglucan production while the rest of the population do not or only weakly contribute. We noted consistent propagation of the contributor state to the descendants implying epigenetic transfer of the regulatory state to the next generation.

Our data showed a lack of significant correlation between expression of the galactoglucan biosynthesis operon and the AHL synthase gene *sinI* although AHL-bound ExpR has been reported as a strong transcriptional activator of galactoglucan biosynthesis and a moderate activator of *sinI* expression (Charoenpanich et al., 2013; McIntosh et al., 2008). This indicates that under the growth conditions applied in this study QS-dependent regulation cannot be the sole source of heterogeneity in *wgeA* promoter activation. Apart from QS, other regulatory inputs have been reported including MucR, a zinc finger-type transcriptional repressor, and PhoB mediating phosphate limitation-dependent regulation (Bahlawane et al., 2008a,b; Rüberg et al., 1999).

Activity of the *sinI* promoter displayed heterogeneity in the early phase of colony development while at later stages, an overall activation of P*sinI* was observed in virtually all individuals. This is best explained by the initial occurrence of some QS active individuals while the remaining individuals of the colony show no QS activity. At later time points an increase in AHL signal molecule concentration probably triggers more and more individuals into the QS state. QS activation is strongly dependent on environmental conditions such as nutrient availability and population density (McIntosh et al., 2009). In *S. fredii* NGR234 populations, promoters of the AHL synthase genes *traI* and *ngrI* showed highly heterogeneous activity patterns during batch culture growth in rich medium. These patterns became more homogeneous after addition of high concentrations of AHLs (Grote et al., 2014). Although, this study and our investigation were performed in different *Sinorhizobium* species under different growth conditions and the former did not provide time lapse data at individual cell level, both suggest the tendency of AHL synthase promoters to behave more homogeneous at high AHL concentrations.

To classify cell types in long-term time lapse studies we tested a novel mathematical strategy based on the increase in fluorescence over time in each individual. In our experimental setup, this strategy proved to be superior over more simple methods only relying on fixed thresholds. We found that considering the time course of signal intensities for individual cells better accounts for biological variance and technical variations in data acquisition. Hence, our improved experimental and data analysis approach represents a useful step forward in expanding the toolbox for elucidation of bacterial phenotypic heterogeneity.

Acknowledgements

This work was supported by grants Be 2121/6-1 and Pf 672/5-1 in the framework of the priority program "Phenotypic Heterogeneity and Sociobiology of Bacterial Populations" (SPP 1617, German Research Foundation) and the LOEWE Program of the State of Hessen (SYNMIKRO). We thank Bernadette Boomers and Andreas Kautz for supporting primary image analysis of colony time lapse data. The mVenus gene used in this study was a gift from Daniella Cavalcanti de Lucena.

Appendix A. Supplementary data

Supplementary data associated with this article can be found, in the online version, at http://dx.doi.org/10.1016/j.jbiotec.2015.01.021.

References

Anetzberger, C., Schell, U., Jung, K., 2012. Single cell analysis of *Vibrio harveyi* uncovers functional heterogeneity in response to quorum sensing signals. BMC Microbiol. 12, 209, http://dx.doi.org/10.1186/1471-2180-12-209.

Arnoldini, M., Vizcarra, I.A., Peña-Miller, R., Stocker, N., Diard, M., Vogel, V., Beardmore, R.E., Hardt, W.-D., Ackermann, M., 2014. Bistable expression of virulence genes in *Salmonella* leads to the formation of an antibiotic-tolerant subpopulation. PLoS Biol. 12, e1001928, http://dx.doi.org/10.1371/journal.pbio.1001928.

Bahlawane, C., Baumgarth, B., Serrania, J., Rüberg, S., Becker, A., 2008a. Fine-tuning of galactoglucan biosynthesis in *Sinorhizobium meliloti* by differential WggR (ExpG)-, PhoB-, and MucR-dependent regulation of two promoters. J. Bacteriol. 190, 3456–3466, http://dx.doi.org/10.1128/JB.00062-08.

Bahlawane, C., McIntosh, M., Krol, E., Becker, A., 2008b. *Sinorhizobium meliloti* regulator MucR couples exopolysaccharide synthesis and motility. Mol. Plant-Microbe Interact. 21, 1498–1509, http://dx.doi.org/10.1094/MPMI-21-11-1498.

Bartels, F.W., Baumgarth, B., Anselmetti, D., Ros, R., Becker, A., 2003. Specific binding of the regulatory protein ExpG to promoter regions of the galactoglucan biosynthesis gene cluster of *Sinorhizobium meliloti*—a combined molecular biology and force spectroscopy investigation. J. Struct. Biol. 143, 145–152.

Baumgarth, B., Bartels, F.W., Anselmetti, D., Becker, A., Ros, R., 2005. Detailed studies of the binding mechanism of the *Sinorhizobium meliloti* transcriptional activator ExpG to DNA. Microbiol. Read. Engl. 151, 259–268, http://dx.doi.org/10.1099/mic.0.27442-0.

Beaumont, H.J.E., Gallie, J., Kost, C., Ferguson, G.C., Rainey, P.B., 2009. Experimental evolution of bet hedging. Nature 462, 90–93, http://dx.doi.org/10.1038/nature08504.

Becker, A., Rüberg, S., Baumgarth, B., Bertram-Drogatz, P.A., Quester, I., Pühler, A., 2002. Regulation of succinoglycan and galactoglucan biosynthesis in *Sinorhizobium meliloti*. J. Mol. Microbiol. Biotechnol. 4, 187–190.

Becker, A., Rüberg, S., Küster, H., Roxlau, A.A., Keller, M., Ivashina, T., Cheng, H.P., Walker, G.C., Pühler, A., 1997. The 32-kilobase exp gene cluster of *Rhizobium meliloti* directing the biosynthesis of galactoglucan: genetic organization and properties of the encoded gene products. J. Bacteriol. 179, 1375–1384.

Buendia, A.M., Enenkel, B., Köplin, R., Niehaus, K., Arnold, W., Pühler, A., 1991. The *Rhizobium meliloti exoZI exoB* fragment of megaplasmid 2: ExoB functions as a UDP-glucose 4-epimerase and ExoZ shows homology to NodX of *Rhizobium leguminosarum* biovar *viciae* strain TOM. Mol. Microbiol. 5, 1519–1530.

Casadesús, J., Low, D.A., 2013. Programmed heterogeneity: epigenetic mechanisms in bacteria. J. Biol. Chem. 288, 13929–13935, http://dx.doi.org/10.1074/jbc.R113.472274.

Chai, Y., Chu, F., Kolter, R., Losick, R., 2008. Bistability and biofilm formation in *Bacillus subtilis*. Mol. Microbiol. 67, 254–263, http://dx.doi.org/10.1111/j.1365-2958.2007.06040.x.

Charoenpanich, P., Meyer, S., Becker, A., McIntosh, M., 2013. Temporal expression program of quorum sensing-based transcription regulation in *Sinorhizobium meliloti*. J. Bacteriol. 195, 3224–3236, http://dx.doi.org/10.1128/JB.00234-13.

Charoenpanich, P., Soto, M.J., Becker, A., McIntosh, M., 2014. Quorum sensing restrains growth and is rapidly inactivated during domestication of *Sinorhizobium meliloti*. Environ. Microbiol. Rep., http://dx.doi.org/10.1111/1758-2229.12262 [Epub ahead of print].

Chastanet, A., Vitkup, D., Yuan, G.-C., Norman, T.M., Liu, J.S., Losick, R.M., 2010. Broadly heterogeneous activation of the master regulator for sporulation in *Bacillus subtilis*. Proc. Natl. Acad. Sci. U.S.A. 107, 8486–8491, http://dx.doi.org/10.1073/pnas.1002499107.

Dhar, N., McKinney, J.D., 2007. Microbial phenotypic heterogeneity and antibiotic tolerance. Curr. Opin. Microbiol. 10, 30–38, http://dx.doi.org/10.1016/j.mib.2006.12.007.

Dunlop, M.J., Cox, R.S., Levine, J.H., Murray, R.M., Elowitz, M.B., 2008. Regulatory activity revealed by dynamic correlations in gene expression noise. Nat. Genet. 40, 1493–1498, http://dx.doi.org/10.1038/ng.281.

Elowitz, M.B., Levine, A.J., Siggia, E.D., Swain, P.S., 2002. Stochastic gene expression in a single cell. Science 297, 1183–1186, http://dx.doi.org/10.1126/science.1070919.

EMD Millipore Corporation, 2014. User Guide CellASIC® ONIX B04A-03 Microfluidic Bacteria Plates. EMD Millipore Corporation.

Fagerlund, A., Dubois, T., Økstad, O.-A., Verplaetse, E., Gilois, N., Bennaceur, I., Perchat, S., Gominet, M., Aymerich, S., Kolstø, A.-B., Lereclus, D., Gohar, M., 2014. SinR controls enterotoxin expression in *Bacillus thuringiensis* biofilms. PLoS ONE 9, e87532, http://dx.doi.org/10.1371/journal.pone.0087532.

Frunzke, J., Bramkamp, M., Schweitzer, J.-E., Bott, M., 2008. Population Heterogeneity in *Corynebacterium glutamicum* ATCC 13032 caused by prophage CGP3. J. Bacteriol. 190, 5111–5119, http://dx.doi.org/10.1128/JB.00310-08.

Gao, M., Coggin, A., Yagnik, K., Teplitski, M., 2012. Role of specific quorum-sensing signals in the regulation of exopolysaccharide II production within *Sinorhizobium meliloti* spreading colonies. PLoS ONE 7, e42611, http://dx.doi.org/10.1371/journal.pone.0042611.

Galibert, F., Finan, T.M., Long, S.R., Pühler, A., Abola, P., Ampe, F., Barloy-Hubler, F., Barnett, M.J., et al., 2001. The composite genome of the legume symbiont *Sinorhizobium meliloti*. Science 293, 668–672.

Glenn, S.A., Gurich, N., Feeney, M.A., González, J.E., 2007. The ExpR/Sin quorum-sensing system controls succinoglycan production in *Sinorhizobium meliloti*. J. Bacteriol. 189, 7077–7088, http://dx.doi.org/10.1128/JB.00906-07.

González, J.E., Marketon, M.M., 2003. Quorum sensing in nitrogen-fixing rhizobia. Microbiol. Mol. Biol. Rev. 67, 574–592.

Grant, S.G., Jessee, J., Bloom, F.R., Hanahan, D., 1990. Differential plasmid rescue from transgenic mouse DNAs into *Escherichia coli* methylation-restriction mutants. Proc. Natl. Acad. Sci. U.S.A. 87, 4645–4649.

Grote, J., Krysciak, D., Schorn, A., Dahlke, R.I., Soonvald, L., Müller, J., Hense, B.A., Schwarzfischer, M., Sauter, M., Schmeisser, C., Streit, W.R., 2014. Evidence of autoinducer-dependent and -independent heterogeneous gene expression in *Sinorhizobium fredii* NGR234. Appl. Environ. Microbiol. 80, 5572–5582, http://dx.doi.org/10.1128/AEM.01689-14.

Grünberger, A., Wiechert, W., Kohlheyer, D., 2014. Single-cell microfluidics: opportunity for bioprocess development. Curr. Opin. Biotechnol. 29C, 15–23, http://dx.doi.org/10.1016/j.copbio.2014.02.008.

Ham, T.S., Lee, S.K., Keasling, J.D., Arkin, A.P., 2006. A tightly regulated inducible expression system utilizing the fim inversion recombination switch. Biotechnol. Bioeng. 94, 1–4, http://dx.doi.org/10.1002/bit.20916.

Helaine, S., Kugelberg, E., 2014. Bacterial persisters: formation, eradication, and experimental systems. Trends Microbiol. 22, 417–424, http://dx.doi.org/10.1016/j.tim.2014.03.008.

Huang, C.T., Xu, K.D., McFeters, G.A., Stewart, P.S., 1998. Spatial patterns of alkaline phosphatase expression within bacterial colonies and biofilms in response to phosphate starvation. Appl. Environ. Microbiol. 64, 1526–1531.

Huang, C.T., Yu, F.P., McFeters, G.A., Stewart, P.S., 1995. Nonuniform spatial patterns of respiratory activity within biofilms during disinfection. Appl. Environ. Microbiol. 61, 2252–2256.

Jones, K.M., Kobayashi, H., Davies, B.W., Taga, M.E., Walker, G.C., 2007. How rhizobial symbionts invade plants: the *Sinorhizobium–Medicago* model. Nat. Rev. Microbiol. 5, 619–633, http://dx.doi.org/10.1038/nrmicro1705.

Khan, S.R., Gaines, J., Roop, R.M., Farrand, I.I.S.K., 2008. Broad-host-range expression vectors with tightly regulated promoters and their use to examine the influence of TraR and TraM expression on Ti plasmid quorum sensing. Appl. Environ. Microbiol. 74, 5053–5062, http://dx.doi.org/10.1128/AEM.01098-08.

Lehman, A.P., Long, S.R., 2013. Exopolysaccharides from *Sinorhizobium meliloti* can protect against H_2O_2-dependent damage. J. Bacteriol. 195, 5362–5369, http://dx.doi.org/10.1128/JB.00681-13.

Lipniacki, T., Paszek, P., Marciniak-Czochra, A., Brasier, A.R., Kimmel, M., 2006. Transcriptional stochasticity in gene expression. J. Theor. Biol. 238, 348–367, http://dx.doi.org/10.1016/j.jtbi.2005.05.032.

Maisonneuve, E., Gerdes, K., 2014. Molecular mechanisms underlying bacterial persisters. Cell 157, 539–548, http://dx.doi.org/10.1016/j.cell.2014.02.050.

McIntosh, M., Krol, E., Becker, A., 2008. Competitive and cooperative effects in quorum-sensing-regulated galactoglucan biosynthesis in *Sinorhizobium meliloti*. J. Bacteriol. 190, 5308–5317, http://dx.doi.org/10.1128/JB.00063-08.

McIntosh, M., Meyer, S., Becker, A., 2009. Novel *Sinorhizobium meliloti* quorum sensing positive and negative regulatory feedback mechanisms respond to phosphate availability. Mol. Microbiol. 74, 1238–1256, http://dx.doi.org/10.1111/j.1365-2958.2009.06930.x.

Miao, H., Ratnasingam, S., Pu, C.S., Desai, M.M., Sze, C.C., 2009. Dual fluorescence system for flow cytometric analysis of *Escherichia coli* transcriptional response in multi-species context. J. Microbiol. Methods 76, 109–119, http://dx.doi.org/10.1016/j.mimet.2008.09.015.

Müller, J., Kuttler, C., Hense, B.A., Zeiser, S., Liebscher, V., 2008. Transcription, intercellular variability and correlated random walk. Math. Biosci. 216, 30–39, http://dx.doi.org/10.1016/j.mbs.2008.08.003.

Nagai, T., Ibata, K., Park, E.S., Kubota, M., Mikoshiba, K., Miyawaki, A., 2002. A variant of yellow fluorescent protein with fast and efficient maturation for cell-biological applications. Nat. Biotechnol. 20, 87–90, http://dx.doi.org/10.1038/nbt0102-87.

Neumeyer, A., Hübschmann, T., Müller, S., Frunzke, J., 2013. Monitoring of population dynamics of *Corynebacterium glutamicum* by multiparameter flow cytometry. Microb. Biotechnol. 6, 157–167, http://dx.doi.org/10.1111/1751-7915.12018.

Okumus, B., Yildiz, S., Toprak, E., 2014. Fluidic and microfluidic tools for quantitative systems biology. Curr. Opin. Biotechnol. 25, 30–38, http://dx.doi.org/10.1016/j.copbio.2013.08.016.

Pedraza, J.M., van Oudenaarden, A., 2005. Noise propagation in gene networks. Science 307, 1965–1969, http://dx.doi.org/10.1126/science.1109090.

Pellock, B.J., Teplitski, M., Boinay, R.P., Bauer, W.D., Walker, G.C., 2002. A LuxR homolog controls production of symbiotically active extracellular polysaccharide II by *Sinorhizobium meliloti*. J. Bacteriol. 184, 5067–5076.

Pérez, J., Jiménez-Zurdo, J.I., Martínez-Abarca, F., Millán, V., Shimkets, L.J., Muñoz-Dorado, J., 2014. Rhizobial galactoglucan determines the predatory pattern of *Myxococcus xanthus* and protects *Sinorhizobium meliloti* from predation. Environ. Microbiol. 16, 2341–2350, http://dx.doi.org/10.1111/1462-2920.12477.

Pradhan, B.B., Chatterjee, S., 2014. Reversible non-genetic phenotypic heterogeneity in bacterial quorum sensing. Mol. Microbiol. 92, 557–569, http://dx.doi.org/10.1111/mmi.12575.

Ratcliff, W.C., Denison, R.F., 2010. Individual-level bet hedging in the bacterium *Sinorhizobium meliloti*. Curr. Biol. CB 20, 1740–1744, http://dx.doi.org/10.1016/j.cub.2010.08.036.

Ratcliff, W.C., Denison, R.F., 2011. Bacterial persistence and bet hedging in *Sinorhizobium meliloti*. Commun. Integr. Biol. 4, 98–100, http://dx.doi.org/10.4161/cib.4.1.14161.

Rinaudi, L.V., Sorroche, F., Zorreguieta, Á., Giordano, W., 2010. Analysis of the *mucR* gene regulating biosynthesis of exopolysaccharides: implications for biofilm formation in *Sinorhizobium meliloti* Rm1021. FEMS Microbiol. Lett. 302, 15–21, http://dx.doi.org/10.1111/j.1574-6968.2009.01826.x.

Rizzo, M.A., Springer, G.H., Granada, B., Piston, D.W., 2004. An improved cyan fluorescent protein variant useful for FRET. Nat. Biotechnol. 22, 445–449, http://dx.doi.org/10.1038/nbt945.

Rowat, A.C., Bird, J.C., Agresti, J.J., Rando, O.J., Weitz, D.A., 2009. Tracking lineages of single cells in lines using a microfluidic device. Proc. Natl. Acad. Sci. U.S.A. 106, 18149–18154, http://dx.doi.org/10.1073/pnas.0903163106.

Rüberg, S., Pühler, A., Becker, A., 1999. Biosynthesis of the exopolysaccharide galactoglucan in *Sinorhizobium meliloti* is subject to a complex control by the phosphate-dependent regulator PhoB and the proteins ExpG and MucR. Microbiol. Read. Engl. 145 (Pt 3), 603–611.

Sanchez-Romero, M.A., Casadesús, J., 2014. Contribution of phenotypic heterogeneity to adaptive antibiotic resistance. Proc. Natl. Acad. Sci. U.S.A. 111, 355–360, http://dx.doi.org/10.1073/pnas.1316084111.

Serra, D.O., Hengge, R., 2014. Stress responses go three dimensional—the spatial order of physiological differentiation in bacterial macrocolony biofilms. Environ. Microbiol. 16, 1455–1471, http://dx.doi.org/10.1111/1462-2920.12483.

Shaner, N.C., Campbell, R.E., Steinbach, P.A., Giepmans, B.N.G., Palmer, A.E., Tsien, R.Y., 2004. Improved monomeric red, orange and yellow fluorescent proteins derived from *Discosoma* sp. red fluorescent protein. Nat. Biotechnol. 22, 1567–1572, http://dx.doi.org/10.1038/nbt1037.

Simon, R., Priefer, U., Pühler, A., 1983. A broad host range mobilization system for in vivo genetic engineering: transposon mutagenesis in Gram negative bacteria. Nat. Biotechnol. 1, 784–791, http://dx.doi.org/10.1038/nbt1183-784.

Solopova, A., van Gestel, J., Weissing, F.J., Bachmann, H., Teusink, B., Kok, J., Kuipers, O.P., 2014. Bet-hedging during bacterial diauxic shift. Proc. Natl. Acad. Sci. U.S.A. 111, 7427–7432, http://dx.doi.org/10.1073/pnas.1320063111.

Stewart, M.K., Cookson, B.T., 2012. Non-genetic diversity shapes infectious capacity and host resistance. Trends Microbiol. 20, 461–466, http://dx.doi.org/10.1016/j.tim.2012.07.003.

Stewart, P.S., Franklin, M.J., 2008. Physiological heterogeneity in biofilms. Nat. Rev. Microbiol. 6, 199–210, http://dx.doi.org/10.1038/nrmicro1838.

Tauch, A., Zheng, Z., Pühler, A., Kalinowski, J., 1998. *Corynebacterium striatum* chloramphenicol resistance transposon Tn5564: genetic organization and transposition in *Corynebacterium glutamicum*. Plasmid 40, 126–139, http://dx.doi.org/10.1006/plas.1998.1362.

Tokunaga, M., Imamoto, N., Sakata-Sogawa, K., 2008. Highly inclined thin illumination enables clear single-molecule imaging in cells. Nat. Methods 5, 159–161, http://dx.doi.org/10.1038/nmeth1171.

Veening, J.-W., Hamoen, L.W., Kuipers, O.P., 2005. Phosphatases modulate the bistable sporulation gene expression pattern in *Bacillus subtilis*. Mol. Microbiol. 56, 1481–1494, http://dx.doi.org/10.1111/j.1365-2958.2005.04659.x.

Veening, J.-W., Smits, W.K., Hamoen, L.W., Kuipers, O.P., 2006. Single cell analysis of gene expression patterns of competence development and initiation of sporulation in *Bacillus subtilis* grown on chemically defined media. J. Appl. Microbiol. 101, 531–541, http://dx.doi.org/10.1111/j.1365-2672.2006.02911.x.

Veening, J.-W., Smits, W.K., Kuipers, O.P., 2008. Bistability, epigenetics, and bet-hedging in bacteria. Annu. Rev. Microbiol. 62, 193–210, http://dx.doi.org/10.1146/annurev.micro.62.081307.163002.

Von Bodman, S.B., Willey, J.M., Diggle, S.P., 2008. Cell–cell communication in bacteria: united we stand. J. Bacteriol. 190, 4377–4391, http://dx.doi.org/10.1128/JB.00486-08.

Weaver, W.M., Tseng, P., Kunze, A., Masaeli, M., Chung, A.J., Dudani, J.S., Kittur, H., Kulkarni, R.P., Di Carlo, D., 2014. Advances in high-throughput single-cell microtechnologies. Curr. Opin. Biotechnol. 25, 114–123, http://dx.doi.org/10.1016/j.copbio.2013.09.005.

Wentland, E.J., Stewart, P.S., Huang, C.T., McFeters, G.A., 1996. Spatial variations in growth rate within *Klebsiella pneumoniae* colonies and biofilm. Biotechnol. Prog. 12, 316–321, http://dx.doi.org/10.1021/bp9600243.

Zhan, H.J., Lee, C.C., Leigh, J.A., 1991. Induction of the second exopolysaccharide (EPSb) in *Rhizobium meliloti* SU47 by low phosphate concentrations. J. Bacteriol. 173, 7391–7394.